Oxidation of GaN: An *ab initio* thermodynamic approach

Adam J. Jackson and Aron Walsh*
Centre for Sustainable Chemical Technologies & Department of Chemistry, University of Bath, BA2 7AY Bath, United Kingdom
(Received 19 June 2013; revised manuscript received 5 August 2013; published 11 October 2013)

GaN is a wide-band-gap semiconductor used in high-efficiency light-emitting diodes and solar cells. The solid is produced industrially at high chemical purities by deposition from a vapor phase, and oxygen may be included at this stage. Oxidation represents a potential path for tuning its properties without introducing more exotic elements or extreme processing conditions. In this work, *ab initio* computational methods are used to examine the energy potentials and electronic properties of different extents of oxidation in GaN. Solid-state vibrational properties of Ga, GaN, Ga_2O_3, and a single substitutional oxygen defect have been studied using the harmonic approximation with supercells. A thermodynamic model is outlined which combines the results of *ab initio* calculations with data from experimental literature. This model allows free energies to be predicted for arbitrary reaction conditions within a wide process envelope. It is shown that complete oxidation is favorable for all industrially relevant conditions, while the formation of defects can be opposed by the use of high temperatures and a high N_2:O_2 ratio.

DOI: 10.1103/PhysRevB.88.165201 PACS number(s): 82.33.Pt, 82.60.−s, 71.15.Mb

I. INTRODUCTION

Solid-state lighting with light-emitting diodes (LEDs) offers exceptionally high efficiencies, and systems with luminous efficacies of over 100 $\mathrm{lmW^{-1}}$ are already commercially available.[1] With experimental systems achieving up to 169 $\mathrm{lmW^{-1}}$, researchers are continuing to move performance toward the theoretical limit for white light of around 300 $\mathrm{lmW^{-1}}$ (depending on the definition of "white").[2] GaN, in pure and indium-doped forms, has been an instrumental part of this movement, forming many of the highest-performing LED systems.

Very pure semiconductors such as GaN are generally formed under high vacuum by techniques including chemical vapor deposition (CVD) and molecular beam epitaxy (MBE). Such conditions require specialized equipment and considerable energy. It would be desirable to carry out deposition reactions at more modest pressures, but this risks the presence of gas impurities and may make the system more difficult to control. In particular, oxygen is thought to form solid solutions with GaN, substituting N atoms for O at low concentrations (<30%) and altering the resistivity and band gap—important properties for its electronic applications.[3] A temperature of 500 °C is considered "low-temperature" for deposition and 800–1000 °C is more typical; this coincides with the maximum solubility of oxygen.[3] A recent attempt at atomic layer deposition of GaN at modest temperatures (<400 °C) obtained a bulk oxygen concentration of 19.5%.[4]

However, it has also been reported that higher temperatures can reduce the concentration of gallium oxide by controlling the rate of deposition; Obinata *et al*. attribute the formation of Ga-O bonds to a film of "excess Ga," but they also note that gallium oxide existed within their GaN films.[5] A proposed solution is annealing in the presence of ammonia, providing excess nitrogen.[6]

In addition to the growth process, GaN is known to thermally decompose under vacuum at temperatures above around 700 °C (i.e., reaction conditions), with a strong temperature dependence, and this is also suppressed by nitrogen.[7] The thermodynamic significance of varying nitrogen pressures is therefore of interest.

A range of material modeling techniques have been applied to GaN in the past. These include analytical pairwise potential[8,9] and electronic structure studies.[10–13] The computational defect physics was reviewed by Neugebauer and Van de Walle,[14] while Zywietz *et al*. investigated the incorporation of oxygen on the material surface.[15]

The key reaction considered in this study was the oxidation of GaN under formation conditions. Complete oxidation is expected to occur at high temperatures, above typical deposition conditions:

$$2\mathrm{GaN} + \tfrac{3}{2}\mathrm{O_2} \rightarrow \mathrm{Ga_2O_3} + \mathrm{N_2},$$

while the dominant form of oxidation at deposition conditions is the substitution of N atoms for O at low concentrations:

$$\mathrm{N_N} + \tfrac{1}{2}\mathrm{O_2} \rightarrow \mathrm{O_N} + \tfrac{1}{2}\mathrm{N_2}.$$

GaN adopts the wurtzite crystal structure with tetrahedral ion coordination environments; this is represented by a small hexagonal unit cell, whereas the stable β structure of Ga_2O_3 corresponds to a more complex monoclinic unit cell, with both tetrahedral and octahedral elements (Fig. 1).

II. METHODOLOGY

The aim of the study was to predict the envelope of conditions for thermodynamically stable GaN and free energies of several degrees of oxidation. This is achieved by using density functional theory (DFT) to calculate the energies of pure and defective compounds.[16,17] Energy minimization with DFT is based purely on the electronic potential field, and does not account directly for any lattice vibrations, or the effect of pressure. By adding the zero-point vibrational energy E^{ZP} to the DFT-derived energy E^{DFT}, we can obtain an energy value which we define as equivalent to various thermodynamic potentials at zero temperature and zero pressure (indicated with a superscript 0):

$$\begin{aligned} G^0 &= H^0 = U^0 \\ &= E^0_{\mathrm{potential}} + E^0_{\mathrm{vibrational}} = E^{\mathrm{DFT}} + E^{\mathrm{ZP}}, \end{aligned} \quad (1)$$

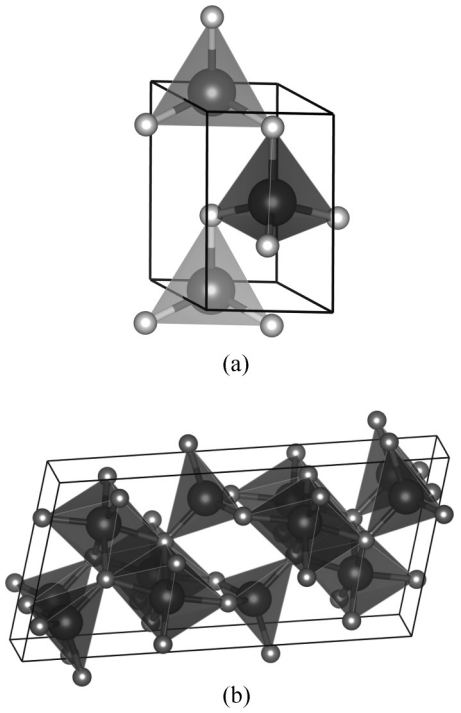

FIG. 1. Unit cell with bounding box for (a) GaN and (b) β-Ga_2O_3: dark spheres represent Ga atoms and lighter spheres show the position of N (a) and O (b) atoms.

where G, H, and U are the Gibbs free energy, enthalpy, and internal energy, respectively. The contributions of individual components may be considered in terms of their chemical potentials μ_i. For ideal materials, the chemical potential is equivalent to the Gibbs free energy of one unit (i.e., 1 mole) of the pure material, and hence

$$\mu_i^0 = G_i^0 = E_i^{\mathrm{DFT}} + E_i^{\mathrm{ZP}}. \quad (2)$$

Introducing the chemical potential at given reaction conditions $\mu_i(T,p)$, and rearranging,

$$\mu_i(T,p) = E_i^{\mathrm{DFT}} + E_i^{\mathrm{ZP}} + \left[\mu_i(T,p) - \mu_i^0\right]. \quad (3)$$

A slightly different approach is needed to collect this information for each material. In the solid phase, E_i^{DFT} is calculated for crystalline unit cells with a three-dimensional periodic boundary condition. E_i^{ZP} and the free-energy change with temperature and pressure $[\mu_i(T,p) - \mu_i^0]$ require some combination of approximations, literature data, and/or lattice dynamics calculations.[18]

In the gas phase, the DFT energy for an isolated molecule must be found in a method consistent with the solid component energies. Zero-point and free energies are readily available in the literature for common gases such as O_2 and N_2, although care must be taken to use consistent reference points.

A. Total energies and structures

DFT calculations were carried out using the Fritz Haber Institute *ab initio* molecular simulations (FHI-AIMS) package.[19] FHI-AIMS is highly scalable across thousands of computer cores[20] and uses atom-centered numerically tabulated basis sets to describe all of the electrons in the system. All energies and structures were converged using the provided "tight" or "tier 2" basis set, which includes hydrogen-like s, p, d, and f atomic orbitals for Ga and adds a g orbital for N and O. With the exception of molecular oxygen, all calculations did not include spin polarization. The PBEsol exchange-correlation functional was selected; this functional uses the generalized gradient approximation (GGA) and is intended for solid-state calculations.[21,22] The use of the GGA for examining the electronic structures of semiconductors has been challenged recently as it tends to underestimate formation energies and band gaps; nonetheless, PBEsol is considered to offer a good balance of accuracy and efficiency for total energies and structure optimization.[23,24]

1. Pure compounds

Initial crystal structures for GaN, β-Ga_2O_3, and Ga metal were obtained from the literature via the Chemical Database Service at Daresbury and the Inorganic Crystal Structure Database (ICSD).[25–27] The unit-cell parameters and atomic positions were converged with FHI-AIMS and PBEsol to give energies (E^{DFT}) of the pure compounds. The geometry optimization routine was permitted to vary both the cell content and unit-cell parameters in order to minimize the overall energy. The routine employs analytical stress tensors with an adapted Broyden-Fletcher-Shanno-Goldfarb (BFGS) algorithm.[19] The relaxed unit-cell parameters are given in Table I. $\boldsymbol{k}$-points were defined as an evenly spaced grid in reciprocal space, centered on the Γ point, and time-reversal symmetry was employed to reduce the required number of calculations. The $\boldsymbol{k}$-point-grid density was scaled to the unit-cell size to achieve uniform sampling with a target length cutoff of 10 Å, as described by Moreno and Soler.[28]

Oxygen (in the triplet spin configuration) and nitrogen gases were modeled by setting an isolated pair of atoms 1 Å

TABLE I. Relaxed structure parameters from DFT calculations with FHI-AIMS and the PBEsol functional. $\boldsymbol{k}$-points are sampled evenly in reciprocal space and include the Γ-point. Lengths are in Å and angles are in degrees. For diatomic gases, a is the distance between the nuclei.

	Initial parameters							Relaxed structure					
Compound	a	b	c	α	β	γ	$\boldsymbol{k}$-points	a	b	c	α	β	γ
GaN (Ref. 25)	3.189	3.189	5.186	90	90	120	[774]	3.186	3.186	5.187	90.01	89.99	120.07
Ga_2O_3 (Ref. 26)	12.214	3.037	5.798	90	103.83	90	[284]	12.287	3.049	5.812	90.00	103.72	90.00
Ga	4.520	7.660	4.526	90	90	90	[646]	4.424	7.605	4.532	90.01	90.00	90.00
O_2	1.000							1.212					
N_2	1.000							1.101					

TABLE II. Zero-point energies, standard enthalpies, and bond lengths (r) for diatomic gases from the literature.[31,32]

Material	E^{ZP} (eV)	E^{ZP} (kJ mol^{-1})	$[H^\theta - H^0]$ (kJ mol^{-1})	r (Å)
O_2	0.0976	9.42	8.680	1.2075
N_2	0.1458	14.07	8.670	1.0977

apart and allowing them to relax to a distance minimizing the energy. The resulting distances are also included in Table I, each overestimating their recorded spectroscopic value by 1% (Table II).

2. Defects

Dilute oxidation in bulk GaN was modeled by the supercell approach: 72-atom, 128-atom, and 300-atom supercells were created from the relaxed hexagonal 4-atom GaN unit cell as described in Appendix A. Energies were calculated with and without a single substitution of an N atom for an O atom. The atomic positions within the cell were relaxed to find an energy minimum using the BFGS algorithm as above.

To model the dilute limit of oxidation, it is necessary here to apply a band-filling correction. Oxygen substitution in GaN results in an excess electron that occupies the conduction band. As the defect concentration decreases, the conduction-band filling drops to the band minimum, usually at the Γ point. A correction energy was calculated by integrating over the eigenvalues above this reference energy for each $\boldsymbol{k}$-point, following the method described by Persson *et al.*[29] and discussed in more detail by Lany and Zunger.[30] This has been implemented as a MATLAB routine, available on request.

B. Gases—Literature data

Gas properties in *ab initio* thermodynamics can be calculated using statistical mechanics, but in practice they are generally drawn from experimental values.[33–35] In this case, properties for O_2 and N_2 were calculated using data from standard thermochemical tables, which have been fitted by NIST to polynomial equations of the form developed by Shomate.[39–42] Such correlations are especially convenient for use in computer programs. The correction for temperature and pressure in Eq. (3), $[\mu_i(T,p) - \mu_i^0]$, requires a reference state of zero, while the majority of data in the literature are relative to standard conditions of 298.15 K and 1 bar. It is therefore convenient to break up the correction to use this reference state, which is denoted with a superscript θ:

$$\mu_i(T,p_i) = E_i^{DFT} + E_i^{ZP} + \left[\mu_i(T,p_i) - \mu_i^\theta\right] + \left[\mu_i^\theta - \mu_i^0\right]. \tag{4}$$

Introducing the relationship with enthalpy, $\mu_i = H_i - TS$,

$$\mu_i^\theta - \mu_i^0 = \left[H_i^\theta - (TS)^\theta\right] - \left[H_i^0 - (TS)^0\right]. \tag{5}$$

$(TS)^0 = 0$, so simplifying and rearranging,

$$\mu_i^\theta - \mu_i^0 = \left[H_i^\theta - H_i^0\right] - (TS)^\theta. \tag{6}$$

Substituting this back into Eq. (4),

$$\mu_i(T,p_i) = E_i^{DFT} + E_i^{ZP} + \left[\mu_i(T,p_i) - \mu_i^\theta\right] + \left[H_i^\theta - H_i^0\right] - (TS)^\theta. \tag{7}$$

Of these terms, E_i^{DFT} is found by *ab initio* calculations, E_i^{ZP} depends on the vibrational frequencies and is relatively small (literature values are given in Table II), and $[H_i^\theta - H_i^0]$ and $(TS)^\theta = 298.15\ \text{K} \times S^\theta$ are available from the literature data. The only variable term is $[\mu_i(T,p_i) - \mu_i^\theta]$. Introducing the group $\mu_i(T,p_i^\theta)$ to break the process into isothermal pressure change and isobaric temperature change,

$$\left[\mu_i(T,p_i) - \mu_i^\theta\right] = \left[\mu_i(T,p_i) - \mu_i(T,p_i^\theta)\right] + \left[\mu_i(T,p_i^\theta) - \mu_i^\theta\right]. \tag{8}$$

To account for the pressure change, we use an ideal-gas relationship,[43]

$$\left[\mu_i(T,p_i) - \mu_i\left(T,p_i^\theta\right)\right] = RT\ln\left(p_i/p_i^\theta\right), \tag{9}$$

$$\left[\mu_i(T,p_i) - \mu_i^\theta\right] = RT\ln\left(p_i/p_i^\theta\right) + \left[\mu_i\left(T,p_i^\theta\right) - \mu_i^\theta\right]. \tag{10}$$

The temperature change uses the standard constant-pressure heat capacity $C_p(T) = \left(\frac{\partial H}{\partial T}\right)_{p^\theta}$,

$$\left[\mu_i\left(T,p_i^\theta\right) - \mu_i^\theta\right] = \left[H_i\left(T,p_i^\theta\right) - H_i^\theta\right] - \left[TS\left(T,p_i^\theta\right) - T^\theta S^\theta\right], \tag{11}$$

$$\left[\mu_i\left(T,p_i^\theta\right) - \mu_i^\theta\right] = \int_{T^\theta}^{T} C_p dT - \left[TS\left(T,p_i^\theta\right) - T^\theta S^\theta\right]. \tag{12}$$

Combining Eqs. (7), (10), and (12),

$$\mu_i(T,p_i) = E^{DFT} + E^{ZP} + RT\ln\left(p_i/p_i^\theta\right) + \int_{T^\theta}^{T} C_p dT - \left[TS\left(T,p_i^\theta\right) - T^\theta S^\theta\right] + \left[H_i^\theta - H_i^0\right] - (TS)^\theta, \tag{13}$$

TABLE III. Thermal properties from phonon calculations with FHI-AIMS and PHONOPY: zero-point energy E^{ZP}, standard Helmholtz free energy $A^{298.15\ K}$, and standard heat capacity $C_p^{298.15\ K}$.

			Unit-cell basis			Formula unit basis		
Compound	Supercell	$\boldsymbol{k}$-points	E^{ZP} (eV)	$A^{298.15\ K}$ (eV)	$C_p^{298.15\ K}$ (k_B)	E^{ZP} (kJmol^{-1})	$A^{298.15\ K}$ (kJmol^{-1})	$C_p^{298.15\ K}$ (Jmol^{-1}K^{-1})
GaN	[332]	[333]	0.305	0.217	8.529	14.70	10.45	35.46
Ga	[222]	[323]	0.194	−0.356	23.069	2.34	−4.29	23.98
Ga_2O_3	[132]	[232]	1.412	0.933	44.597	34.07	22.50	92.70
$Ga_{36}N_{35}O$	[332]	[111]	5.410	3.791	154.715	521.94	365.76	1286.37

$$\mu_i(T,p_i) = \underbrace{E^{\mathrm{DFT}} + E^{\mathrm{ZP}}}_{\text{Energy at zero}} + \underbrace{\left[H_i^\theta - H_i^0\right]}_{\text{Standard enthalpy}} + \underbrace{\int_{T^\theta}^{T} C_p dT}_{\text{Enthalpy correction}} + \underbrace{RT\ln\left(p_i/p_i^\theta\right)}_{\text{Free-energy correction}} - \underbrace{TS\left(T,p_i^\theta\right)}_{\text{Entropic contribution}}. \quad (14)$$

The key pieces of data needed are therefore the standard enthalpy, $[H_i^\theta - H_i^0]$, the heat capacity, C_p, and the entropy, S, as functions of temperature at standard pressure. The standard enthalpy is available from reference books, while the temperature-dependent heat capacity and entropy are obtained from tables or polynomial equations as discussed above.

C. Lattice dynamics

Thermal properties were calculated within the harmonic approximation using the PHONOPY 1.5 software package, preparing and post-processing FHI-AIMS calculations.[36] The number of $\boldsymbol{k}$-points was scaled to match the 10 Å target length cutoff employed in relaxation calculations. Forces were calculated for atomic displacements of 0.01 Å, with a convergence threshold of 1×10^{-5} eV Å^{-1}.

PHONOPY follows the Parlinski-Li-Kawazoe method to generate a "dynamical matrix" of forces describing the harmonic behavior of the atoms in the system. In this scheme the second derivatives of energy are obtained by combining analytical first derivatives with small displacements in supercells.[37] These second derivatives yield a set of phonon frequencies, ω, which may be expressed as a phonon band structure and density of states (DOS).[18] Ultimately a thermodynamic partition function can be formed for each mode,

$$Z_i = \sum_j \exp\left(\frac{E_j}{k_B T}\right), \quad (15)$$

where the energy at a given state $E_j = \hbar\omega_j$; the product of all Z_i yields an overall partition function Z from which the Helmholtz free energy is calculated,

$$A = -k_B T \ln Z. \quad (16)$$

This energy includes the zero-point energy at 0 K, and by differentiation the heat capacity, entropy, and related properties are obtained as functions of temperature. In this study, the relationship was sampled over temperature with a density of at least one point per degree Kelvin, and any intermediate values were estimated using cubic spline interpolation.

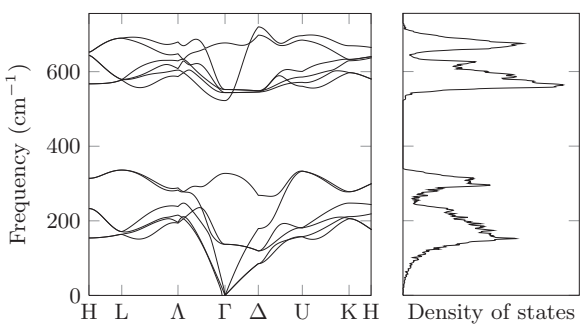

FIG. 2. Phonon band structure and density of states for GaN.

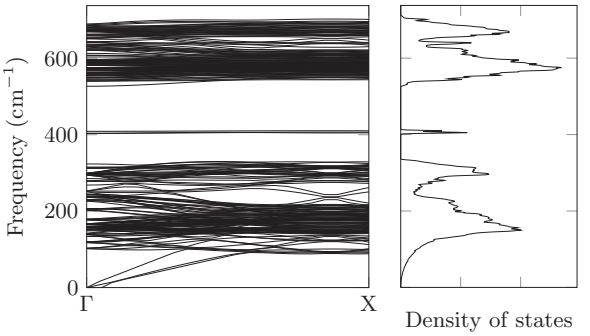

FIG. 3. Phonon band structure and density of states for $Ga_{36}N_{35}O$.

It is possible to use the quasiharmonic approximation to account for the influence of pressure and thermal expansion by modeling compressed and expanded supercells; GaN is relatively incompressible, with a bulk modulus of over 200 GPa, and in this study the effect is assumed to be negligible.[38] A higher level of accuracy can be obtained with use of molecular-dynamics (MD) simulations with an appropriate thermostat. The computational cost of this approach is very high, as many time steps are needed to obtain a converged statistical average. Nonetheless, the approach accounts for higher-order anharmonicity, within the scope of the analytical potentials or *ab initio* method used to calculate energies and forces.

Given a suitable function for heat capacity, it is possible to expand Eq. (3) and calculate the chemical potentials of known crystals under an absolute pressure P,

$$\mu_i(T,P) = E_i^{\mathrm{DFT}} + E_i^{\mathrm{ZP}} + \int_0^T C_p dT + PV - TS_{\mathrm{vib}}(T), \quad (17)$$

where E^{ZP}, $C_p(T)$, and the vibrational entropy contribution $S_{\mathrm{vib}}(T)$ are drawn from the dynamic lattice model, and PV is simply the total pressure multiplied by the specific volume.

D. Derivation of free energy

The materials are assumed to be ideal in that the chemical potentials μ_i of each component i in isolation may simply be summed together to obtain the overall Gibbs free energy of

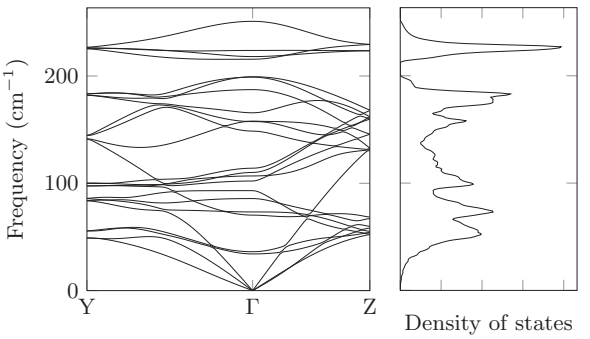

FIG. 4. Phonon band structure and density of states for Ga.

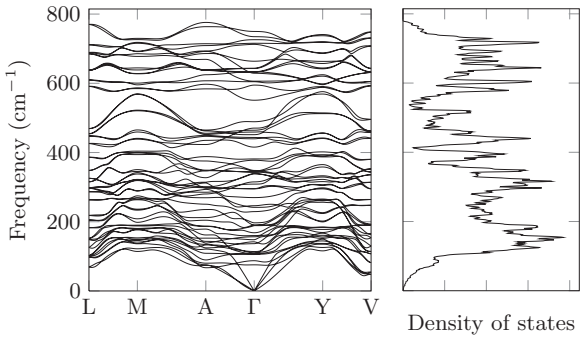

FIG. 5. Phonon band structure and density of states for Ga_2O_3.

reaction, ΔG_r,

$$\Delta G_r(T,P) = \sum_i \mu_i(T,p)\Delta n_i, \tag{18}$$

where T is the temperature, P is the total system pressure, p is the partial pressure of a component, and Δn_i is the stoichiometric change for the component i. A more advanced model might substitute the partial pressures for fugacities.

III. RESULTS

A. Bulk thermodynamic properties

1. Solid-state thermodynamic potentials

The lattice dynamic calculations described in Sec. II C were applied to relaxed structures of Ga, GaN, and Ga_2O_3 to obtain free energies, entropies, and heat capacities. The dispersion curve and DOS for GaN show similar behavior to work based on analytical potential models and Raman spectroscopy,[49–51] while the Ga_2O_3 curves may be compared to a previous *ab initio* study.[52] Two defect-containing supercells were also subjected to this analysis: the 72- and 128-atom supercells in which one nitrogen atom is substituted for oxygen, i.e., $Ga_{36}N_{35}O$ and $Ga_{64}N_{63}O$. The calculated zero-point energies are given with standard-temperature Helmholtz free energies ($A = U - TS$) and heat capacities in Table III, and phonon band structures in Figs. 2–5. The temperature variation of entropy is presented in Fig. 6: on an atomic basis, the values for the oxygen and nitrogen compounds are relatively close, while the Ga metal has greater entropy. The overall defect entropy

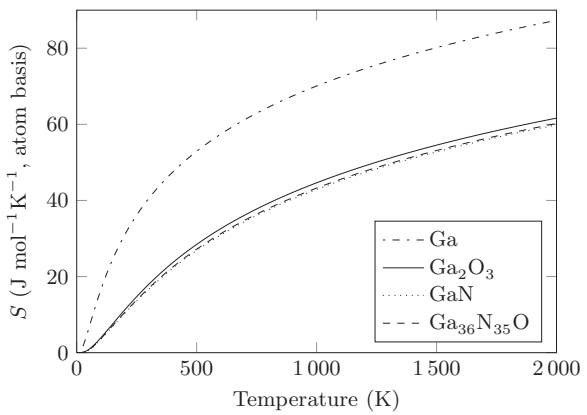

FIG. 6. Solid-state vibrational entropies from phonon calculations.

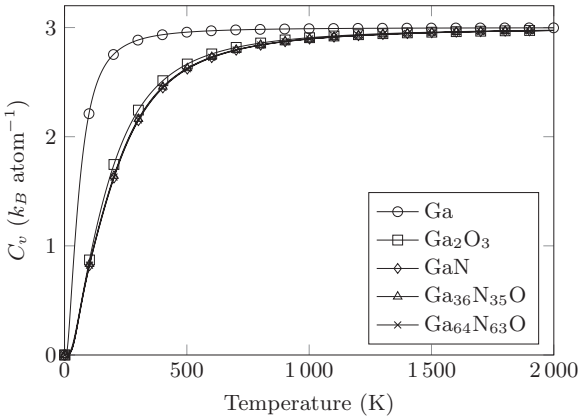

FIG. 7. Solid-state heat capacities from phonon calculations.

change appears to be of the order of 25 Jmol^{-1} K^{-1}; this is comparable with other work on point defects in ionic compounds, and corresponds to a non-negligible amount of energy at high temperatures.[53,54]

2. Heat capacities

All computed heat capacities are given over the studied temperature range in Fig. 7; the behavior of the gallium compounds is extremely close, and all materials tend toward the Dulong-Petit limit of $3k_B$ per atom.

Comparing these results with the literature, the *ab initio* heat capacity of GaN is plotted against several fits to experimental data in Fig. 8. Danilchenko *et al.* fitted a mixed Debye and Einstein model to data from low-temperature calorimetry, while Leitner *et al.* carried out high-temperature measurements and formed an empirical model including data from other researchers.[46] Jacob *et al.* used differential scanning calorimetry (DSC) to return a slightly lower set of high-temperature heat capacity data.[45] Not shown is the result of Sanati and Estreicher's *ab initio* calculation, which used a Ceperley-Alder local-density functional at a single $\boldsymbol{k}$-point, and it appears to

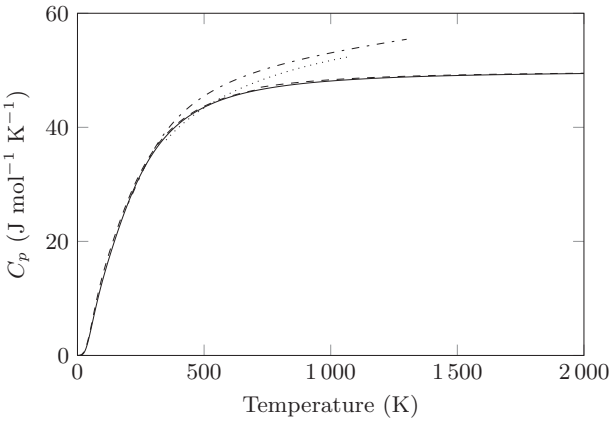

FIG. 8. Heat capacity for GaN: (–) PBEsol or harmonic approximation; (- -) Debye–Einstein fit to adiabatic calorimetry measurements, Danilchenko *et al.*[44]; (· · ·) DSC measurements and empirical fit by Jacob *et al.*[45]; (- · -) fit by Leitner *et al.*, incorporating data from Calvet calorimetry and other literature.[46]

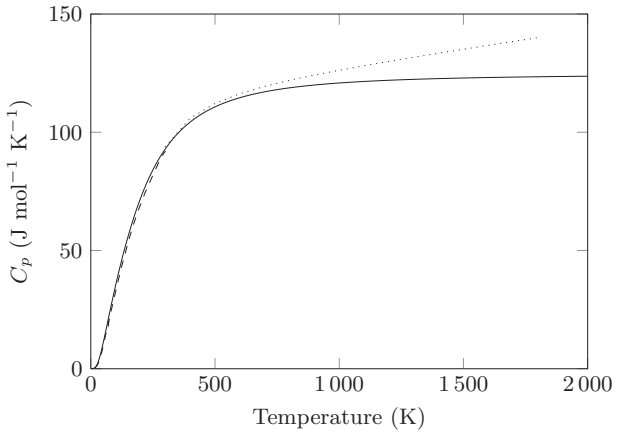

FIG. 9. Heat capacity for Ga_2O_3: (–) PBEsol with harmonic approximation; (- -) low temperature calorimetry data from Adams[47]; (· · ·) high-temperature calorimetry from Mills.[48]

give similar results to ours.[55] Of interest is the fact that the systems based on theory (phonon integration and Debye and Einstein models) tend toward the Dulong-Petit limit, while the experimental and empirical work exceeds this limit. The simple harmonic approaches do not account for electronic and anharmonic contributions, which may yield this additional heat capacity. In addition to the deviations in heat capacity, it is worth bearing in mind that Ga is molten above around 300 K, and simple thermal decomposition of GaN is not taken into account: these are reference states rather than physical models.

The heat capacity of Ga_2O_3 shows similar behavior relative to the literature, with a close correspondence at low temperatures and deviation from around 500 K (Fig. 9). The phonon band structures for GaN (Figs. 2 and 3) clearly show the impact of the defect; a cluster of three "gap bands" appears at around 400 cm^{-1}, providing a set of vibrational energies which are available at lower temperatures than the optic modes above 500 cm^{-1}. These correspond to highly localized vibrations of the substitutional oxygen atom. The effect manifests itself as a peak in the difference in heat capacity of pure and

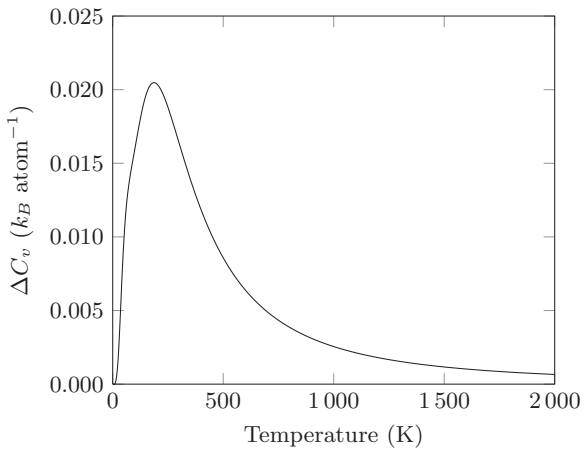

FIG. 10. Difference in heat capacity between pure GaN and a 72-atom supercell with single oxygen substitution: $\Delta C_v = C_{v,\mathrm{Ga_{36}N_{35}O}} - C_{v,36\mathrm{GaN}}$.

TABLE IV. Predicted and experimental enthalpies of formation.[32]

Material	$\Delta H^{\mathrm{calculated}}$ (kJ mol^{-1})	$\Delta H^{\mathrm{experimental}}$ (kJ mol^{-1})
GaN	−112.49	−110
Ga_2O_3	−921.64	−1089.1

oxygen-doped GaN (Fig. 10). The impact of the defect is both qualitatively logical and quantitatively negligible. Given the comparatively small contribution of the heat capacity to the free energy, it should generally be an acceptable approximation to use the heat capacity of the host material in thermodynamic models.

3. *Enthalpy of formation*

Enthalpies of formation at standard conditions were calculated using a simplified form of Eqs. (14) and (18) given that $H = G + TS$:

$$\Delta H_f^\theta = \sum_i (E^{\mathrm{DFT}} + E^{\mathrm{ZPE}} + [H^\theta - H^0])\Delta n_i. \qquad (19)$$

The resulting values are given in Table IV and compared to classic experimental values. While the value for GaN agrees with the literature to within a few kJ mol^{-1}, there is a greater discrepancy for Ga_2O_3. As seen in Figs. 11 and 12, the overall formation enthalpy is dominated by the ground-state potential energy; the common approximation of comparing ground-state energies to standard enthalpy changes could be justified in this case.

While the agreement between this work and the established literature is close, it is worth observing that the standard enthalpy of formation of GaN has been the subject of some debate in recent years: Jacob *et al.* suggested a value of −126.792 kJ mol^{-1} in 2007, Peshek *et al.* obtained −165 kJ mol^{-1} in 2008, and Jacob and Rajitha responded in 2009 with a critical letter and a new value of −129.289 kJ mol^{-1}.[45,56,57]

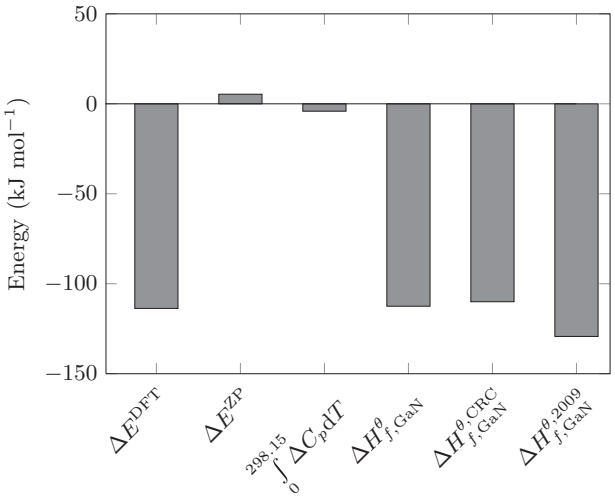

FIG. 11. Contribution of energy terms to overall *ab initio* formation enthalpy of GaN ($\Delta H_{f,\mathrm{GaN}}^{\theta}$) compared to experimental values $\Delta H_{f,\mathrm{GaN}}^{\theta,\mathrm{CRC}}$ and $\Delta H_{f,\mathrm{GaN}}^{\theta,2009}$, from the CRC Handbook and Jacob and Rajita, respectively.[32,57]

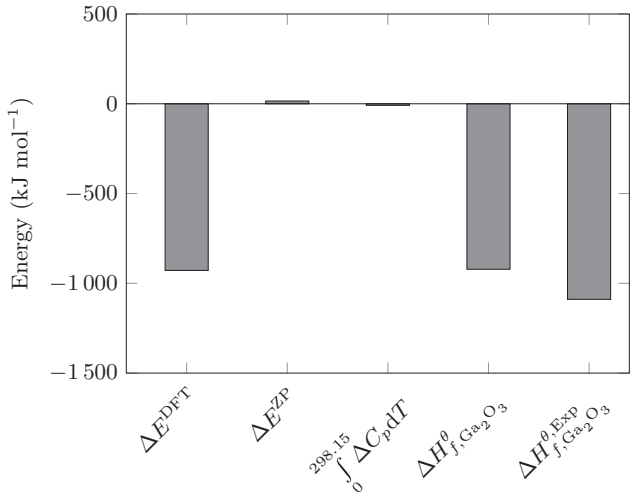

FIG. 12. Contribution of energy terms to overall *ab initio* formation enthalpy of Ga_2O_3 ($\Delta H^{\theta}_{f,\mathrm{Ga_2O_3}}$) compared to the experimental value $\Delta H^{\theta,\mathrm{expt}}_{f,\mathrm{Ga_2O_3}}$.[32]

All of these are greater in magnitude than the value of −110 kJ mol $^{-1}$ reported in the current CRC Handbook of Chemistry and Physics.[32]

B. Complete oxidation

The calculated Gibbs free energy of the oxidation from GaN to Ga_2O_3 is given for a wide range of conditions in Fig. 13. At standard temperature and pressure, with an airlike O_2:N_2 pressure ratio of 20:80, the predicted Gibbs free energy of oxidation is −663.5 kJ mol^{-1}. There is a mild effect of absolute pressure, dropping the energy further by tens of kJ mol^{-1} as demonstrated in Fig. 14, while the relative ratio of gases has a dramatic effect of the order 100 kJ mol^{-1} at elevated temperature (Fig. 13). This is because the entropy of the gas phase decreases at high pressures, and it becomes less unfavorable to remove material to form a solid. At very high pressures (of the order GPa, not shown here) the trend is reversed, but this is beyond the scope of the model as it is driven by the relative compressibilities of gases and solids.

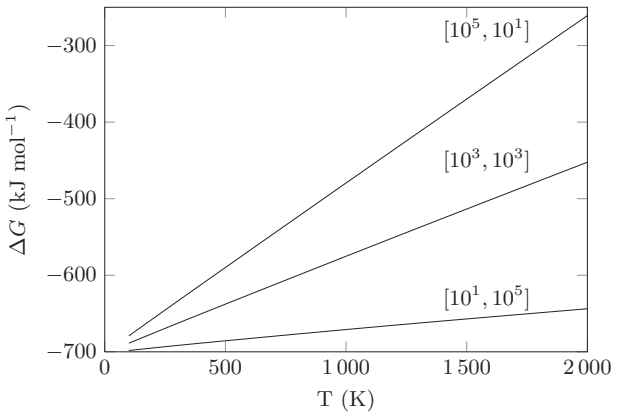

FIG. 13. Modeled Gibbs free energy of complete oxidation from GaN to Ga_2O_3. For each line the corresponding partial pressures, $[pN_2, pO_2]$, are given in Pa.

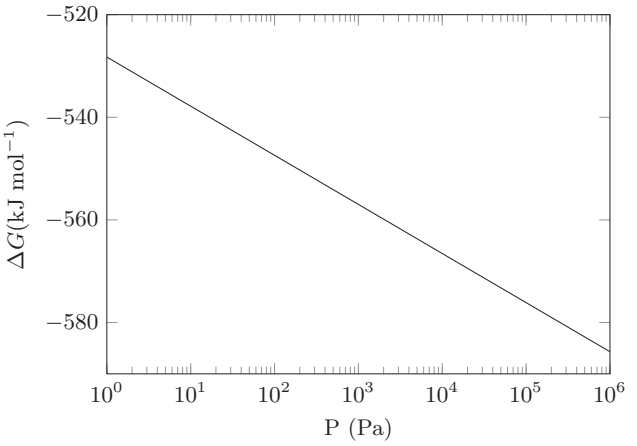

FIG. 14. Modeled Gibbs free energy of complete oxidation from GaN to Ga_2O_3 at 1000 K. Absolute pressure is varied for an atmosphere containing 20%$_{\mathrm{vol}}$ O_2, 80%$_{\mathrm{vol}}$ N_2.

The strongly negative ΔG values indicate that oxidation is favorable at equilibrium under all industrially feasible reaction conditions; the GaN-air system, while temperature-resistant in practice, is not thermodynamically stable. This implies that it relies entirely on kinetic stability.

C. Dilute oxidation

The enthalpies of dilute oxidation (i.e., substitutional oxygen defect formation) can be explored using the energies of large supercells, taking advantage of the relatively small deviation in heat capacity from the pure substance. In Fig. 15, defect formation enthalpies are calculated for standard conditions in an airlike mixture as

$$\Delta H_{\mathrm{defect}} = H_{\mathrm{Ga_xN_{x-1}O}} + 0.5H_{\mathrm{N_2}} - xH_{\mathrm{GaN}} - 0.5H_{\mathrm{O_2}} \qquad (20)$$

and the vibrational contributions to the two solids are assumed to be equivalent as the difference in heat capacity is of the order 0.05 J mol^{-1} K^{-1} (Fig. 10).

The overall defect formation enthalpy is exothermic for all concentrations studied; however, there is a strong dependence

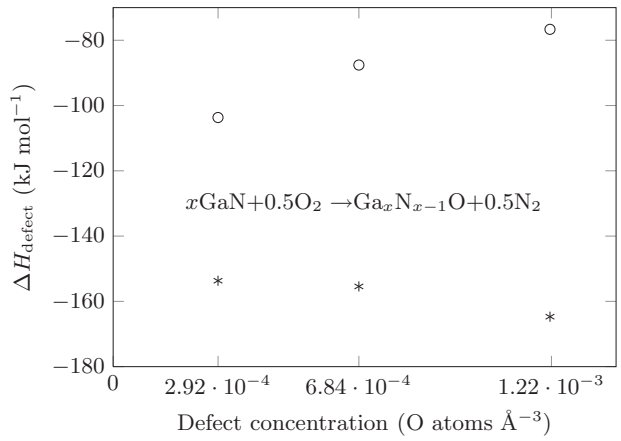

FIG. 15. ○: Enthalpy change (298.15 K, 0.2 bar O_2, 0.8 bar N_2) associated with partial oxidation (single oxygen substitution for GaN supercells); ∗: enthalpy change including band-filling correction (extrapolation to dilute limit).

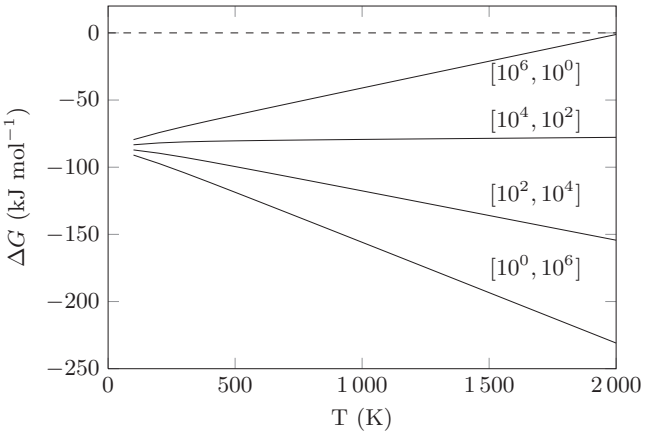

FIG. 16. Modeled Gibbs free energy of partial oxidation from GaN to $Ga_{36}N_{35}O$. For each line the corresponding partial pressures, $[p_{N_2}, p_{O_2}]$, are given in Pa.

on the supercell size, which is varied from $Ga_{36}N_{36}$ to $Ga_{150}N_{150}$. Application of the band-filling correction further stabilizes partial oxidation by ∼40 kJ mol^{-1}, and the values for the two larger supercells appear to approach convergence.

The modeled Gibbs free energy for dilute oxidation is given in Fig. 16 for a single substitution per 72-atom cell over a range of temperatures and partial pressures. At the most extreme conditions the threshold of $\Delta G = 0$ is approached; the operating envelope may be considered more easily as a contour map as in Figs. 17 and 18. Comparing these envelopes for two defect concentrations, we observe that it is actually easier to achieve a positive ΔG for the more dilute defect. The contribution of entropy to the free energy reverses the trend seen for enthalpy in Fig. 15. For example, in the high-pressure high-temperature regime (2000 K, 10^4 bar), the ground-state (ΔE^{DFT}) contributions to Gibbs

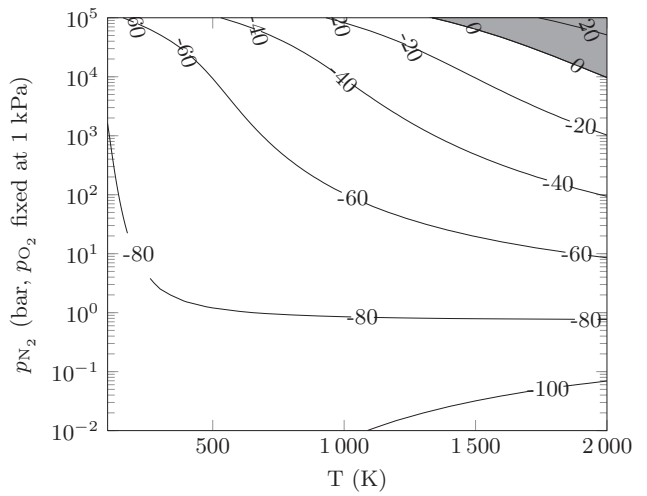

FIG. 17. Gibbs free-energy surface of oxygen defect formation in a 72-atom GaN supercell. Contours are labeled with Gibbs free-energy change (ΔG in kJ mol^{-1}); values above zero (i.e., unfavorable) are shaded.

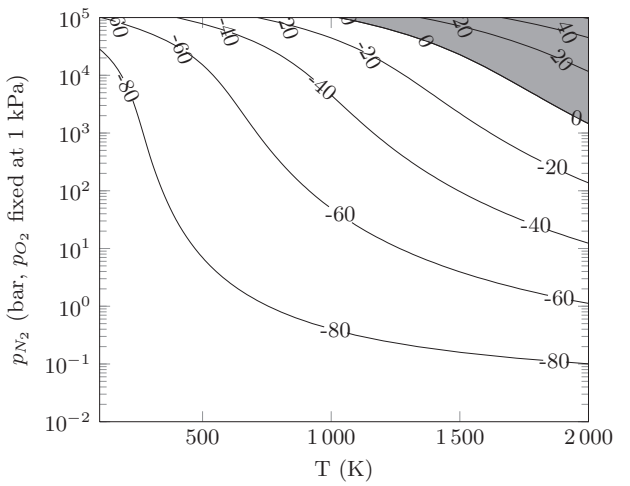

FIG. 18. Gibbs free-energy surface of oxygen defect formation in a 128-atom GaN supercell. Contours are labeled with Gibbs free-energy change (ΔG in kJ mol^{-1}); values above zero (i.e., unfavorable) are shaded.

free energy are −80.7 and −91.6 kJ mol^{-1} for the 72-atom and 128-atom supercells, respectively. In the same region, the entropic $[RT \ln(p_i/p_i^\theta) - TS]$ contributions are −305.6 and −278.0 kJ mol^{-1}. The enthalpy corrections ($\int C_p dT + PV$) of 117.8 and 119.2 kJ mol^{-1} show a smaller concentration dependence.

IV. CONCLUSIONS

A thermodynamic model has been developed for the GaN-O_2-N_2 system from *ab initio* calculations and readily available thermodynamic data. The model permits the free energies and enthalpies of oxidation and defect formation to be calculated for any conditions within a practical processing range. The case of complete oxidation to Ga_2O_3 represents an overall driving force and the behavior following a phase transition, while defect calculations offer insight into the early onset of oxidation.

Varying the ratio of gases provides a strong entropic driving force in the system, and industrial processing conditions are capable of shifting the equilibrium. However, the oxidation of GaN appears to be such a favorable reaction that in practice extreme conditions would be required to prevent oxides or substitutional defects from being thermodynamically stable. The high thermal stability of GaN with respect to oxygen is therefore kinetic in nature.

ACKNOWLEDGMENTS

We thank D. Allsopp for useful discussions. We acknowledge the use of the Chemical Database Service at Daresbury and the Inorganic Crystal Structure Database (ICSD). This work was funded and supported by the EPSRC through the Doctoral Training Centre in Sustainable Chemical Technologies at the University of Bath (EP/G03768X/1). Via our membership of the UK's HPC Materials Chemistry Consortium, which is funded by EPSRC (EP/F067496), this

work made use of the facilities of HECToR, the UK's national high-performance computing service, which is provided by UoE HPCx Ltd. at the University of Edinburgh, Cray Inc., and NAG Ltd., and funded by the Office of Science and Technology through EPSRC's High End Computing Programme. Large structure relaxations and lattice dynamics were calculated using Blue Joule, a Bluegene/Q system at the Science and Technology Facility Council's Daresbury Laboratory, which we were kindly permitted to use as part of the Early Access program.

APPENDIX A: SUPERCELL TRANSFORMATIONS

The transformation matrices in Table V were applied with the VESTA software package[58] to form supercells from the relaxed GaN unit cell.

TABLE V. Generation of supercells from a GaN unit cell.

Atoms in cell	Shape	Transformation matrix
4	Hexagonal	$\begin{pmatrix} 1 & 0 & 0 \\ 0 & 1 & 0 \\ 0 & 0 & 1 \end{pmatrix}$
72	Hexagonal	$\begin{pmatrix} 3 & 0 & 0 \\ 0 & 3 & 0 \\ 0 & 0 & 2 \end{pmatrix}$
128	Orthorhombic	$\begin{pmatrix} 4 & 0 & 0 \\ 2 & 4 & 0 \\ 0 & 0 & 2 \end{pmatrix}$
300	Hexagonal	$\begin{pmatrix} 5 & 0 & 0 \\ 0 & 5 & 0 \\ 0 & 0 & 3 \end{pmatrix}$

*a.walsh@bath.ac.uk

[1] T. W. Murphy, J. Appl. Phys. **111**, 104909 (2012).
[2] Y. Narukawa, M. Ichikawa, D. Sanga, M. Sano, and T. Mukai, J. Phys. D **43**, 354002 (2010).
[3] S. E. Aleksandrov, T. A. Gavrikova, and V. A. Zykov, Semiconductors **34**, 291 (2000).
[4] C. Ozgit, I. Donmez, M. Alevli, and N. Biyikli, J. Vac. Sci. Technol. A **30**, 01A124 (2012).
[5] N. Obinata, K. Sugimoto, K. Ishibiki, S. Egawa, T. Honda, and H. Kawanishi, Jpn. J. Appl. Phys. **44**, 8432 (2005).
[6] M. Sawada, M. Sawadaishi, H. Yamamoto, M. Arai, and T. Honda, J. Cryst. Growth **301–302**, 67 (2007).
[7] S. Fernández-Garrido, G. Koblmüller, E. Calleja, and J. S. Speck, J. Appl. Phys. **104**, 033541 (2008).
[8] P. Zapol, R. Pandey, and J. D. Gale, J. Phys.: Condens. Matter **9**, 9517 (1997).
[9] C. R. A. Catlow, Z. X. Guo, M. Miskufova, S. A. Shevlin, A. G. H. Smith, A. A. Sokol, A. Walsh, D. J. Wilson, and S. M. Woodley, Philos. Trans. R. Soc. London, Ser. A **368**, 3379 (2010).
[10] S. Lany and A. Zunger, Appl. Phys. Lett. **96**, 142114 (2010).
[11] W. R. L. Lambrecht, B. Segall, S. Strite, G. Martin, A. Agarwal, H. Morkoç, and A. Rockett , Phys. Rev. B **50**, 14155 (1994).
[12] S. Limpijumnong, J. E. Northrup, and C. G. Van de Walle, Phys. Rev. B **68**, 075206 (2003).
[13] D. J. Carter, J. D. Gale, B. Delley, and C. Stampfl, Phys. Rev. B **77**, 115349 (2008).
[14] J. Neugebauer and C. G. Van de Walle, Phys. Rev. B **50**, 8067 (1994).
[15] T. K. Zywietz, J. Neugebauer, and M. Scheffler, Appl. Phys. Lett. **74**, 1695 (1999).
[16] P. Hohenberg and W. Kohn, Phys. Rev. **136**, B864 (1964).
[17] W. Kohn and L. Sham, Phys. Rev. **140**, A1133 (1965).
[18] R. P. Stoffel, C. Wessel, M.-W. Lumey, and R. Dronskowski, Angew. Chem. Int. Ed. **49**, 5242 (2010).
[19] V. Blum, R. Gehrke, F. Hanke, P. Havu, V. Havu, X. Ren, K. Reuter, and M. Scheffler, Comput. Phys. Commun. **180**, 2175 (2009).
[20] V. Havu, V. Blum, P. Havu, and M. Scheffler, J. Comput. Phys. **228**, 8367 (2009).
[21] J. P. Perdew, A. Ruzsinszky, G. I. Csonka, O. A. Vydrov, G. E. Scuseria, L. A. Constantin, X. Zhou, and K. Burke, Phys. Rev. Lett. **100**, 136406 (2008).
[22] G. I. Csonka, J. P. Perdew, A. Ruzsinszky, P. H. T. Philipsen, S. Lebègue, J. Paier, O. A. Vydrov, and J. G. Ángyán, Phys. Rev. B **79**, 155107 (2009).
[23] S. Lany, Phys. Rev. B **78**, 245207 (2008).
[24] H. Xiao, J. Tahir-Kheli, and W. A. Goddard, J. Phys. Chem. Lett. **2**, 212 (2011).
[25] W. Paszkowicz, S. Podsiadło, and R. Minikayev, J. Alloys Compd. **382**, 100 (2004).
[26] J. Åhman, G. Svensson, and J. Albertsson, Acta Crystallogr. C **52**, 1336 (1996).
[27] A. Bradley, Z. Kristallogr. **91**, 302 (1935). (Note that due to an apparent error in the ICSD, the initial lattice parameters for Ga deviate slightly from this original source, which gives $a = 4.5167$ Å, $b = 4.5107$ Å, and $c = 7.6448$ Å.)
[28] J. Moreno and J. M. Soler, Phys. Rev. B **45**, 13891 (1992).
[29] C. Persson, Y.-J. Zhao, S. Lany, and A. Zunger, Phys. Rev. B **72**, 035211 (2005).
[30] S. Lany and A. Zunger, Phys. Rev. B **78**, 235104 (2008).
[31] K. K. Irikura, J. Phys. Chem. Ref. Data **36**, 389 (2007).
[32] W. M. Haynes and D. R. Lide, *CRC Handbook of Chemistry and Physics* (Taylor & Francis, London, 2011) .
[33] K. Reuter, C. Stampfl, and M. Scheffler, *Handbook of Materials Modeling, Part A. Methods*, edited by S. Yip (Springer, Berlin, 2005), pp. 149–234.
[34] K. Reuter and M. Scheffler, Phys. Rev. B **65**, 035406 (2001).
[35] B. J. Morgan and G. W. Watson, J. Phys. Chem. C **114**, 2321 (2010).
[36] A. Togo, F. Oba, and I. Tanaka, Phys. Rev. B **78**, 134106 (2008) (PHONOPY is available as an open-source package from http://phonopy.sourceforge.net).
[37] K. Parlinski, Z.-Q. Li, and Y. Kawazoe, Phys. Rev. Lett. **78**, 4063 (1997).
[38] K. Sarasamak, S. Limpijumnong, and W. R. L. Lambrecht, Phys. Rev. B **82**, 035201 (2010).
[39] M. W. J. Chase, *NIST-JANAF Thermochemical Tables* (American Chemical Society, New York, 1998) .
[40] P. Linstrom and W. Mallard, *NIST Chemistry WebBook, Nist Standard Reference Database Number 69* (National Institute of Standards and Technology, Gaithersburg, MD, 2005) .
[41] C. Shomate, J. Am. Chem. Soc. **66**, 928 (1944).
[42] C. Shomate, J. Phys. Chem. **58**, 368 (1954).

[43]J. Warn and A. Peters, *Concise Chemical Thermodynamics*, 2nd ed. (Chapman & Hall, London, 1996), pp. 92–93.
[44]B. A. Danilchenko, T. Paszkiewicz, S. Wolski, A. Jezowski, and T. Plackowski, Appl. Phys. Lett. **89**, 061901 (2006).
[45]K. Jacob, S. Singh, and Y. Waseda, J. Mater. Res. **22**, 3475 (2007).
[46]J. Leitner, A. Strejc, D. Sedmidubský, and K. Růžička, Thermochim. Acta **401**, 169 (2003).
[47]G. B. Adams, Jr. and H. L. Johnston, J. Am. Chem. Soc. **74**, 4788 (1952).
[48]K. Mills, High Temp.-High Pressures **4**, 372 (1972).
[49]T. Azuhata, T. Matsunaga, K. Shimada, K. Yoshida, T. Sota, K. Suzuki, and S. Nakamura, Physica B **219–220**, 493 (1996).
[50]H. Siegle, G. Kaczmarczyk, L. Filippidis, A. P. Litvinchuk, A. Hoffmann, and C. Thomsen, Phys. Rev. B **55**, 7000 (1997).
[51]V. Y. Davydov, Y. E. Kitaev, I. N. Goncharuk, A. N. Smirnov, J. Graul, O. Semchinova, D. Uffmann, M. B. Smirnov, A. P. Mirgorodsky, and R. A. Evarestov, Phys. Rev. B **58**, 12899 (1998).
[52]B. Liu, M. Gu, and X. Liu, Appl. Phys. Lett. **91**, 172102 (2007).
[53]M. J. Gillan and P. W. M. Jacobs, Phys. Rev. B **28**, 759 (1983).
[54]A. Walsh, A. A. Sokol, and C. R. A. Catlow, Phys. Rev. B **83**, 224105 (2011).
[55]M. Sanati and S. K. Estreicher, J. Phys.: Condens. Matter **16**, L327 (2004).
[56]T. J. Peshek, J. C. Angus, and K. Kash, J. Cryst. Growth **311**, 185 (2008).
[57]K. Jacob and G. Rajitha, J. Cryst. Growth **311**, 3806 (2009).
[58]K. Momma and F. Izumi, J. Appl. Crystallogr. **44**, 1272 (2011).